

# Electrochemical Chloride Extraction From Corrosion-Resistant Steel Bar-Reinforced Concrete

Du Fengyin, Jin Zuquan\*, Zhao Tiejun, Dai Xueyan

College of Civil Engineering, Qingdao University of Technology, Qingdao, China

\*E-mail: [jinzquan@126.com](mailto:jinzquan@126.com)

Received: 10 March 2018 / Accepted: 18 April 2018 / Published: 5 June 2018

---

Chloride ion-contaminated concretes with low-carbon steel bar (LC) and corrosion-resistant steel bars (CR) were studied by electrochemical chloride extraction (ECE). The efficiency of the ECE treatment with different electrolyte solutions, current density, protective cover thickness and concrete type were investigated. Moreover, the microstructures, elements distribution, calcium hydroxide content of the concrete, and the interface zone between steel bars and concrete were observed. When ECE treatment with stainless mesh as the anode was applied in contaminated reinforced concrete, the experimental results indicated that a current density of  $2 \text{ A/m}^2$  and a  $\text{Ca(OH)}_2$  solution are recommended. Increasing the concrete cover and compactness of the reinforced concrete decreased the chloride ion removal efficiency. The differences among the steel bar types on the concrete ECE treatment efficiency was negligible. After ECE treatment, re-passivation of steel bars could occur due to the pH recovery and dense microstructure induced by ECE treatment.

---

**Keywords:** reinforced concrete; electrochemical chloride extraction; corrosion-resistant steel bar; microstructure

## 1. INTRODUCTION

The corrosion of steel bars, contributing to more than 80% of the total damages of reinforced concrete structures from “Corrosion” in 2016, is the main threat to building durability. Chloride ion, the main factor of reinforcement corrosion, often lead to the service-life reduction of reinforced concrete exposed to marine environments[1,2]. In particular, the reinforcement corrosion problems of the 150-year-life Jiaozhou Bay Secondary subsea tunnel and the 100-year design life of another major civil building urgently need to be solved.

Various protective methods, including high-performance concrete, coatings, epoxy-coated reinforced bars, and inhibitors are used to improve durability in new structures[3-8]. Corrosion-resistant steel bars with high corrosion resistance and attractive economy have been examined for

replacing carbon steel bars, possibly as another reliable solution to prevent persistent reinforcing steel corrosion. Mohamed[9] found that the element Cr in corrosion-resistant steel bars could prevent Cl migrating into the bars and slow the corrosion rate, leading to good corrosion resistance capacity. Ai[10] demonstrated that Cr takes part in the passivation process of steel, and the passive films present a bilayer structure with the inner layer enriched by Cr species and the outer layer mainly containing Fe species. Recently, corrosion-resistant steel bars replaced carbon steel bars in pier structures in the Jiaozhou Bay Railway Bridge to improve the durability of the bridge in the marine environment.

For ageing structures, the conventional repair technique must detect corroded areas by potential mapping techniques, determine the chloride ion concentration in the corroded zone, and remove chloride-contaminated concrete[11]. Electrochemical chloride extraction (ECE) is a non-destructive method to prevent rebar corrosion and is becoming widely used because of its low cost, high efficiency and small impact on the environment and surroundings[12,13,14]. In the electrochemical chloride extraction process, a direct current is applied between the reinforcement cathode inside the concrete and an anode that is placed outside the concrete[15]. Successful application of ECE depends mainly on the selection of an appropriate anode system[16,17]. Many studies have demonstrated different anode systems such as thermal sprayed zinc[18,19], titanium anodes[20,21], titanium mesh anodes[22,23], conductive paint[24], and coated overlay anodes[25,26], which are currently available for ECE treatment. Stainless steel mesh has been an advantageous anode material used in ECE systems because of its economic cost, corrosion resistance, excellent electrical conductivity and fine plasticity. Moreover, previous research demonstrated that higher-intensity electrochemical treatment can generate concrete cracks and hydrogen embrittlement in steel bars, which leads to structural instability[27-29]. Different electrolyte solutions affect the chloride ion migration rate and change the concrete properties after ECE[30]. Optimal parameters of ECE treatment are extremely significant for efficiency and structural safety, especially for corrosion-resistant steels. ECE as a promising technique to treat chloride-contaminated concrete has not been widely adopted, partly due to the lack of detailed information on the reasonable parameters of the system.

The aim of this investigation was to propose reasonable ECE parameters to treat chloride-contaminated concrete reinforced with corrosion-resistant steel bars. The microstructure evolution of reinforced concrete treated by ECE was also examined.

## 2. EXPERIMENTATION

### 2.1. Reinforced concrete specimen preparation

P.I.52.5 Portland cement and P.O.42.5 ordinary Portland cement were used to prepare high-strength and medium-strength concrete, respectively. Class I fly ash (Chinese standard GB1596-2005) and S95 GGBS (Chinese standard GB/T18046-2008) were employed to partly replace Portland cement. Crushed granite with a maximum size of 25 mm was used as coarse aggregate, whereas river sand with a fineness modulus of 2.6 was used as the fine aggregate. A polycarboxylic super plasticizer was used, and its dosage was adjusted to keep the slump of fresh concrete in the range of 140 mm to 180 mm. The optimized mixture LF50 mixed with approximately 32% GGBS, 17% fly ash and

w/c=0.35 was identified; the mixture was used for lining the concrete structure of the Jiaozhou Subsea Tunnel[31,32]. The comparative concrete L50 with the same w/c and total cement content with LF50 was prepared. The medium-strength concrete L35 with w/c=0.44 and 410 kg.m<sup>-3</sup> of P.O.42.5 ordinary Portland cement were also prepared for comparison purposes. NaCl, corresponding to 0.3% chloride by weight of concrete, was added to the mixing water to form the chloride-contaminated reinforced concrete. The concrete mixture proportions were listed in Table 1.

**Table 1.** Mix proportions of concretes(kg.m<sup>-3</sup>)

No.	kg.m <sup>-3</sup>					
	Cement	GGBS	Fly ash	Sand	Aggregate	Water
L35	410	0	0	668	1240	182
L50	470	0	0	760	1090	165
LF50	240	150	80	760	1090	165
LF50SP1	240	150	80	760	1090	95

Reinforced concrete specimens with a size of 100 mm×100 mm×200 mm for each mix proportion were cast in the laboratory. Two kinds of reinforcement bars called corrosion-resistant steel bars (CR) and low-carbon steel bars (LC) were used as longitudinal reinforcement of the concrete specimens. The concrete covers of the reinforced concrete specimens were controlled as 25 mm, 35 mm and 45 mm. The chemical composites of reinforcement bars are listed in Table 2.

**Table 2.** The chemical compositions of steel bar(%)

Type	The chemical compositions								
	Fe	C	Si	Mn	P	S	V	Cr	Mo
CR	Bal.	0.01	0.49	1.49	0.01	0.01	0.06	10.36	1.16
LC	Bal.	0.22	0.53	1.44	0.02	0.02	0.04	-	-

**Table 3.** Compressive strength and initial chloride ions content of concretes

No.	Initial chloride ions content /%concrete	Compressive strength /Mpa		
		3d	7d	28d
L35	0.293	20.71	27.08	44.17
L35FS	0.287	16.21	25.87	46.07
L50	0.283	45.35	54.71	57.52
LF50	0.288	42.55	54.38	63.58
LF50SP1	0	41.6	52.6	61.5

The steel bars were cleaned and coated with cement paste, followed by epoxy coating at the concrete-air interface. The surface of the steel bars were polished with 200# sand paper. The steel bars were degreased with acetone prior to being placed in the mould; the effective exposure length of the steel bar was 160 mm. The reinforced concrete samples were cast, placed in the mould at room temperature and then removed after 24 h. All specimens were cured at  $20\pm 3$  °C and 95% relative humidity for 28 days. The compressive concrete strengths for concretes cured for different times and their initial chloride ion content are listed in Table 3.

## 2.2 Electrochemical chloride extraction treatments

After 28 days of curing, the reinforced concrete specimens were water saturated by a vacuum pump. Then, an externally derived cathodic current was applied between the steel bar in the concrete specimen and a stainless mesh. The current density was controlled at  $1 \text{ A/m}^2$ ,  $2 \text{ A/m}^2$ , or  $3 \text{ A/m}^2$ . Distilled water, a saturated  $\text{Ca}(\text{OH})_2$  solution and a saturated  $\text{LiOH}$  solution were used as the electrolytes in the ECE treatments. The electrolyte solution was renewed every 2 days, and 200 ml of the solution was taken from the replaced solution. Figure 1 illustrates a schematic diagram of the samples used for the ECE tests. The stainless mesh anode was immersed in the electrolyte solution placed on the concrete surface. The electrolyte level was kept constant during the current passing periods. Different steel surface cathodic current densities were applied for 35 days.

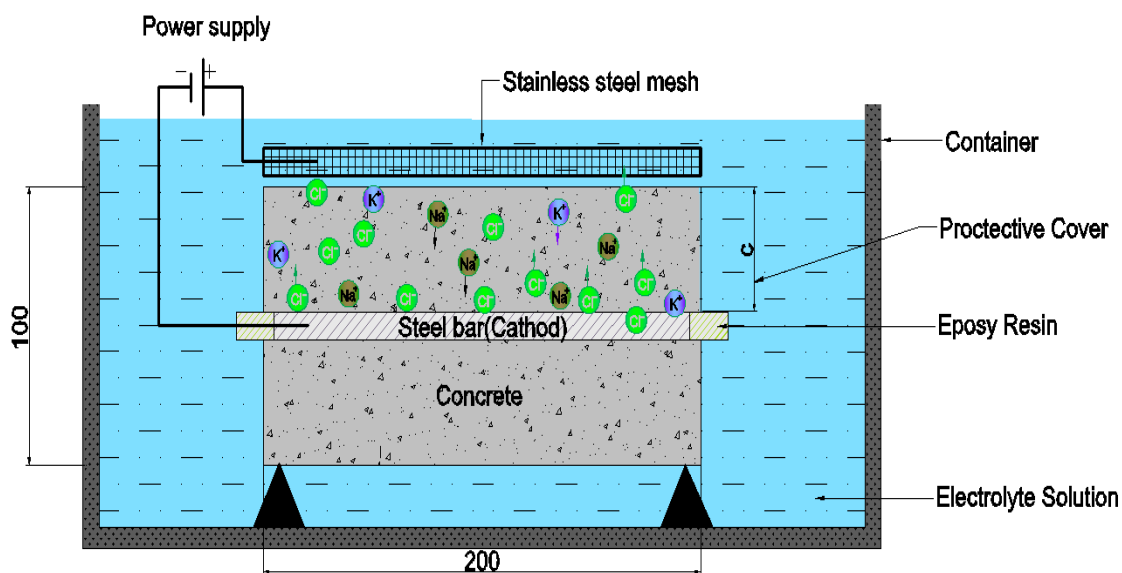


**Figure 1.** Schematic diagram of the samples used for the ECE tests with CCM anode

## 2.3 Determination of the chloride content and microstructure of concrete after ECE

At the end of the ECE treatment, the powder samples were obtained at 2 mm depths from the concrete surface subjected to ECE to the steel bar. Determination of the water-soluble chloride ion

content of the concrete samples was performed by titrating with  $\text{AgNO}_3$  solution [29]. The reinforced concrete specimens after ECE treatment were examined by scanning electron microscopy (SEM) coupled with energy dispersive X-ray spectroscopy (EDS) to determine their microstructure evolution. X-ray Diffraction (XRD) and Differential Scanning Calorimetry-Thermogravimetric Analysis (DSC-TG) were also used to determine the evolution of cement hydration products after ECE treatment.

### 3. RESULTS AND DISCUSSION

#### 3.1 Optimized ECE parameters

The electrochemical chloride extraction was carried out with distilled water, saturated  $\text{Ca}(\text{OH})_2$  solution and saturated  $\text{LiOH}$  solution as the electrolyte solution for C35 concrete with initial chloride ion concentration of 0.29%. From the previous researches[33-35],  $\text{Li}^+$  has some superiority in the inhibition in the alkali-aggregate reaction(AAR) of concrete expansion since the ECE tend to accelerate AAR. The current density was constant at  $2 \text{ A/m}^2$ . The chloride ion content in the solution was measured by chemical titration, and shown in Figure 2. It is obvious that extracted chloride ions content from contaminated reinforced concrete decreased with time, and after 12 days of ECE treatment, the chloride ions content migration from concrete to electrolyte solution kept stable.

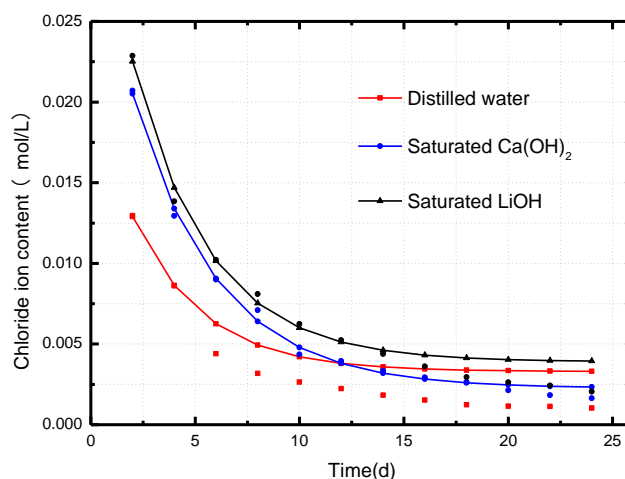


**Figure 2.** Content and fitting results of chloride extracted from different electrolyte solutions

The extracted chloride ion content in the saturated  $\text{LiOH}$  solution was slightly higher than that in the saturated  $\text{Ca}(\text{OH})_2$  solution, while the chlorine removal efficiency of ECE with distilled water as the electrolyte solution continuously remained undesirable and was only approximately 53% of that with the alkali solution. Chang[36] indicated that less bond loss was observed using the  $\text{Ca}(\text{OH})_2$  solution than with the  $\text{NaOH}$  solution. Therefore, using a saturated  $\text{Ca}(\text{OH})_2$  electrolyte solution was recommended when reinforced concrete was mixed with a non-active aggregate.

The chloride ion content extracted from the C35 concrete with the saturated  $\text{Ca}(\text{OH})_2$  electrolyte solution and current densities of  $1 \text{ A/m}^2$ ,  $2 \text{ A/m}^2$ , and  $3 \text{ A/m}^2$  is shown in Figure 3

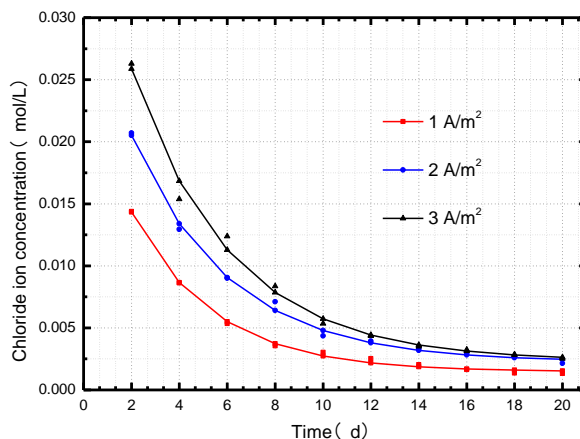


**Figure 3.** Chloride content and fitting results in electrolyte solution after different current densities

More chloride ions were transported from the contaminated reinforced concrete to the electrolyte solution with the higher ECE current density than with the lower current density. However, the relationship between the extracted chloride ion content and the ECE time was fundamentally identical when the current density varied from 1 A/m<sup>2</sup> to 3 A/m<sup>2</sup>.

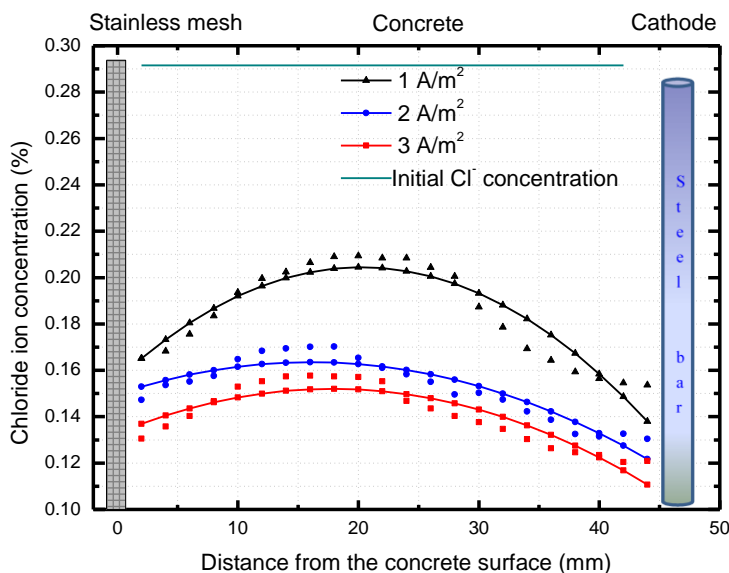


**Figure 4.** Chloride content and quadratic function fitting results for different current densities

After different chlorine current densities were tested, the secondary fitting function of the chloride ion content was calculated as follows:

The chloride ion content profiles after ECE treatment performed on the L35 reinforced concretes with 1-3 A / m<sup>2</sup> for 35 days are shown in Figure 4. The residual chloride ion percentages near the steel bars in the concrete with the ECE current densities of 1, 2, and 3 A / m<sup>2</sup> were 0.16%, 0.13% and 0.12%, respectively. However, the chloride ion content accumulated in the middle of the concrete

cover was 0.21%, 0.16%, and 0.15%, respectively, for the aforementioned current densities. Therefore, the quadratic function was used to describe the relationship between the residual chloride ion levels and the depth in the concrete after ECE treatment, which was as follows.

Fig (b)  $y = -1.17989 \times 10^{-4} x^2 + 0.00478x + 0.15602$  R=0.876

Fig (c)  $y = -5.10462 \times 10^{-5} x^2 + 0.00164x + 0.14901$  R=0.89217

Fig (d)  $y = -6.30285 \times 10^{-5} x^2 + 0.00248x + 0.12719$  R=0.90027

Where x- Distance from the concrete surface (mm)

y- The chloride ion content in concrete (%)

According to the quadratic function, the percentage efficiency of ECE could be calculated using the residual distributions of concrete chloride content compared with the initial concrete chloride content of the cover, which was as follows:

$$E = \left[ 1 - \frac{\int_0^C f(x)dx}{w_0 \times C} \right] \times 100\% \tag{1}$$

Where, E is the chloride ions removal efficiency, C is the distance from steel bar to the surface (mm),  $f(x)$  is the chloride ion distribution function in concrete cover of steel bar, and  $w_0$  is the initial chloride ion content relative to the concrete mass.

The calculated chloride removal efficiency of ECE treatment with different current densities is shown in Figure 5.

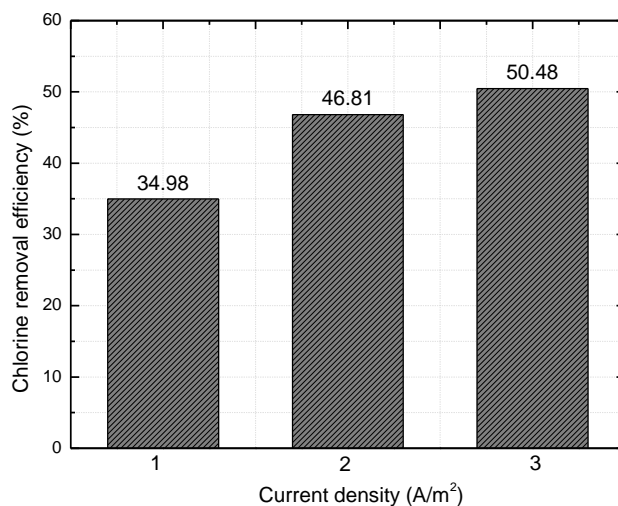


**Figure 5.** Effect of different current densities on chloride removal efficiency

The ECE chloride removal efficiencies with current densities of 1 A/m<sup>2</sup>, 2 A/m<sup>2</sup>, and 3 A/m<sup>2</sup> were 34.98%, 46.81% and 50.48% respectively. The removal efficiencies increased with increasing current density. Previous studies[28,29] verified that higher current density leads to more efficient ECE treatment.

However, when the current density increased from 2 A/m<sup>2</sup> to 3 A/m<sup>2</sup>, the chloride removal efficiency increased by only 7.84%, while the electricity consumption increased by 50%. Additionally, the higher current density for the ECE treatment brought more risk of hydrogen embrittlement of the steel bar within the concrete[27-29]. The authors also believe that higher current densities can generate concrete cracking as a function of the chloride extraction rate[15]. Therefore, 2 A/m<sup>2</sup> was chosen as the suitable value for the ECE treatment. However, the influence of current density on chloride removal efficiency could be ignored 12 days after ECE treatment, and a lower current density could be utilized in the subsequent steps to save cost.

### 3.2 Influences of concrete cover and types of steel bars

C35, C35FS, L50, and LF50 concrete samples with concrete cover thicknesses of 25 mm, 35 mm and 45 mm were used for electrochemical chloride extraction. Concrete specimens were immersed in a saturated Ca(OH)<sub>2</sub> solution, and a cathodic current density of 2 A/m<sup>2</sup> was applied for 30 days. The concrete chloride ion profiles after ECE treatment are shown in Figure 6, and the calculated ECE treatment efficiency is listed in Table 4.

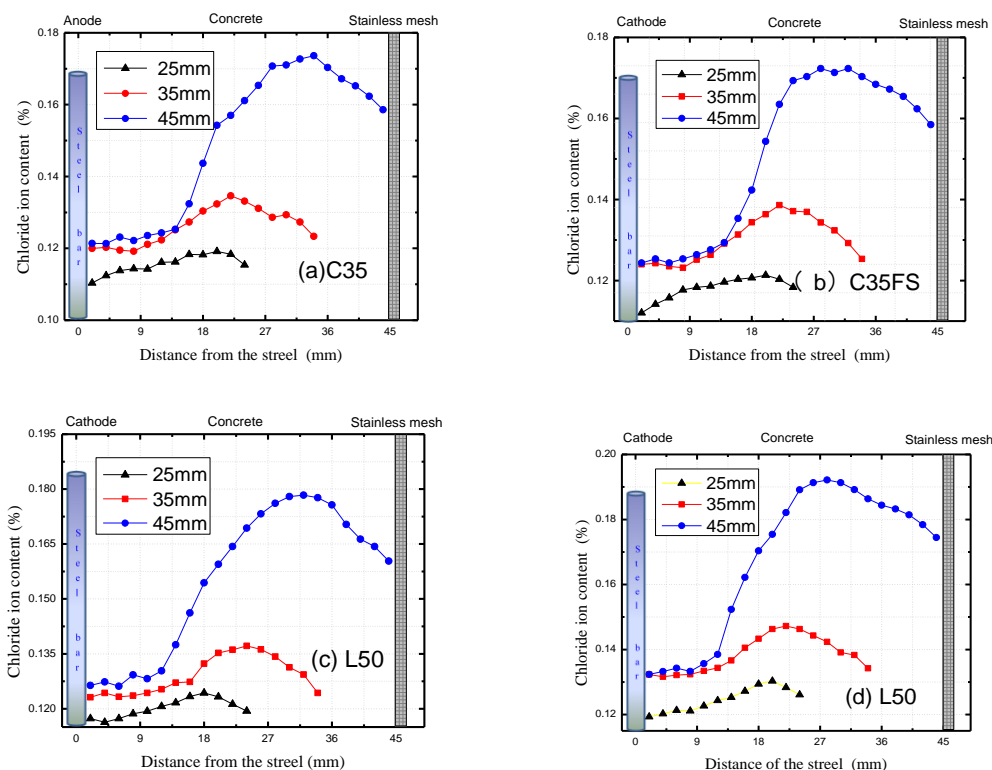


**Figure 6.** Chloride content of concrete with different concrete covers after ECE (a) C35 (b) C35FS (c) L50 (d) LF50

After ECE treatment, the residual chloride ion content in the inner zone 13.5 mm from the steel bar was 40-45% of the initial chloride ion content. The amount of chloride ions accumulated at the surface zone could be observed, and a relatively thicker concrete cover resulted in a significant

increase in the residual chloride ion content in the surface zone of the reinforced concrete. Therefore, the ECE treatment efficiency also decreased with the increasing concrete cover thickness. Moreover, the lower w/b and mineral admixture replacement improved the concrete permeability resistance capacity. Therefore, the imbibition rate of the corroded concrete chloride ions was decreased, and the ECE treatment efficiency was decreased.

The chloride ion content at different depths of concrete reinforced by LC and CR steel bars after ECE treatment is shown in Figure 7.

**Table 4.** ECE treatment efficiency of concrete specimens with different concrete covers depth(%)

	C35	C35FS	L50	LF50
25mm	59.86%	58.07%	56.42%	55.34%
35mm	55.13%	55.68%	57.04%	51.83%
45mm	46.76%	47.94%	46.3%	41.68%

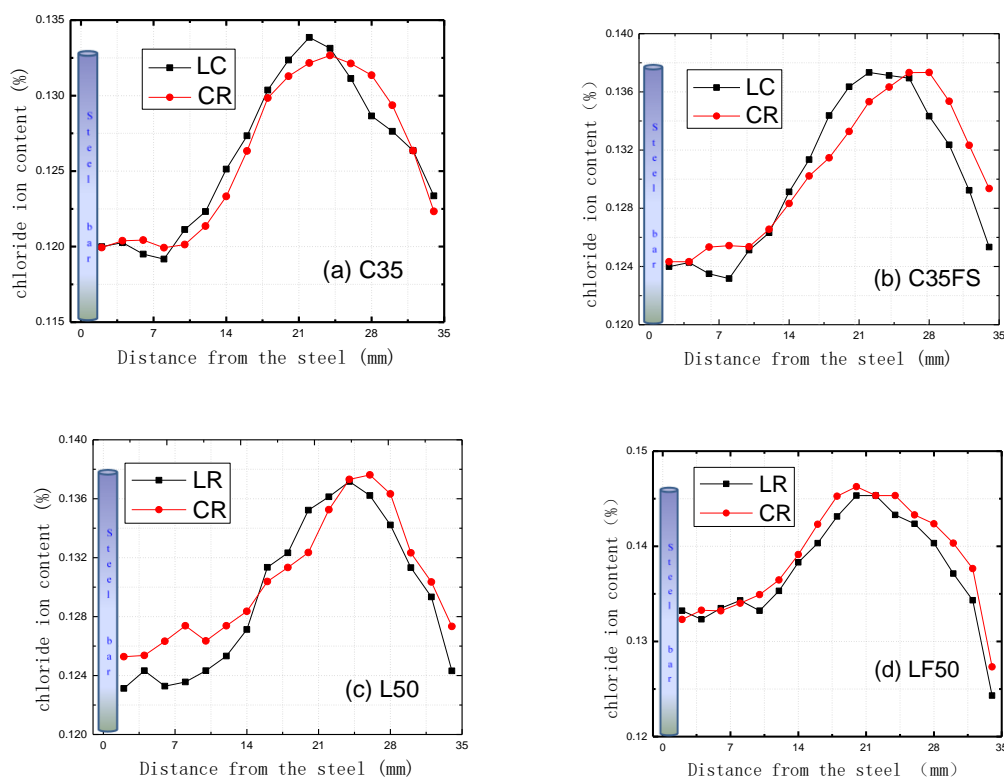


**Figure 7.** Effect of steel type on the chloride removal efficiency (a) C35 (b) C35FS (c) L50 (d) LF50

When the influence of steel bar types on the ECE treatment efficiency was ignored, the chloride removal efficiency was mainly affected by the electrical conductivity of the reinforced concrete, the initial chloride ion content, and the concrete cover. The CR steel bar contained alloy

elements that improved the pitting resistance capacity and increased the critical chloride content. However, since the electrical conductivity of the steel bars did not increase with the addition of an alloy element, the ECE treatment efficiency improvement of CR steel bar reinforced concrete is minimal.

Figure 8 shows the chloride content profiles after ECE treatment performed on the LF50 concrete samples that were exposed in the marine environment for 30 days.

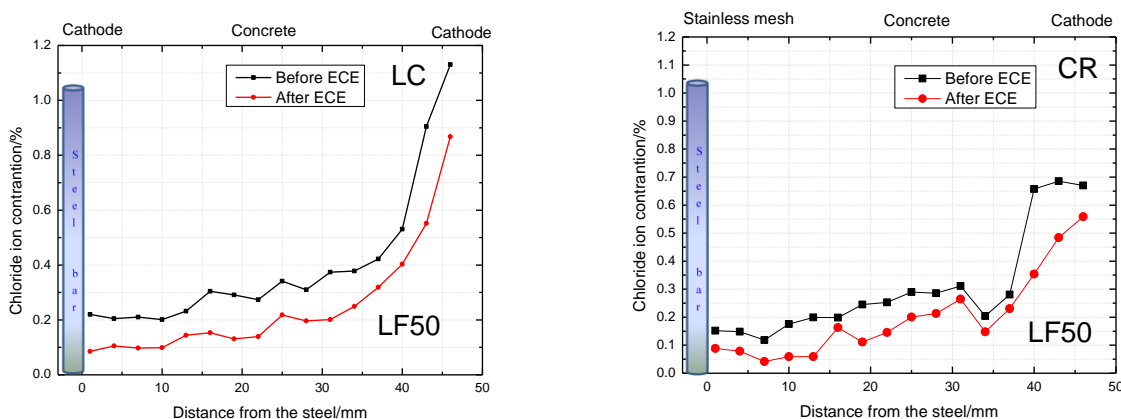


**Figure 8.** Chloride content of concrete exposed to a marine environment with different steel types before and after ECE

Lopez[37] and Arliguie[11] treated samples using concrete cover thicknesses of 20 mm and 50 mm to confirm the results that the thinner cover has better ECE efficiency. More detailed comparisons concerning different parameters of the ECE treatment are shown in Table 5.

**Table.5** Comparisons of chloride reduction in ECE treatment

Reference	anode	Initial Chloride Content (%,by weight of cement)	Current Density	Cover Thickness (mm)	Period (day)	Chloride Reduction(%,near the steel bar)
Fajardo[38]	Titanium	4.60	1.0A/m <sup>2</sup>	50 20	21	30 75
L.R. de Almeida	Stainless steel	1.00	1.0 A/m <sup>2</sup>	10 30	61 (7days rest)	62 55
Souza [15]	mesh	0.45	2.0 A/m <sup>2</sup>	55	33	63
Elsener [28]	Cr-Ni-Steel	1.10			(15 days)	69

	plate				rest)	
Sanchez [29]	Inhibitor solution	1.00	12V	-	90	75
			1	45	20	35
	Stainless steel		2	25	24	59
This paper	steel	0.30	2	35	24	55
	mesh		2	45	24	46
			3	45	20	50

### 3.3 Microstructure of reinforced concrete treated by ECE

The compressive strength of concrete before and after ECE treatment is shown in Fig. 9. The strength loss of C35 and C35FS was approximately 2 MPa, while the compressive strength of L50 and LF50 increased by 0.5 MPa to 1 MPa after ECE treatment. Herein, the influence of ECE treatment on the mechanical properties of the concrete could be ignored.

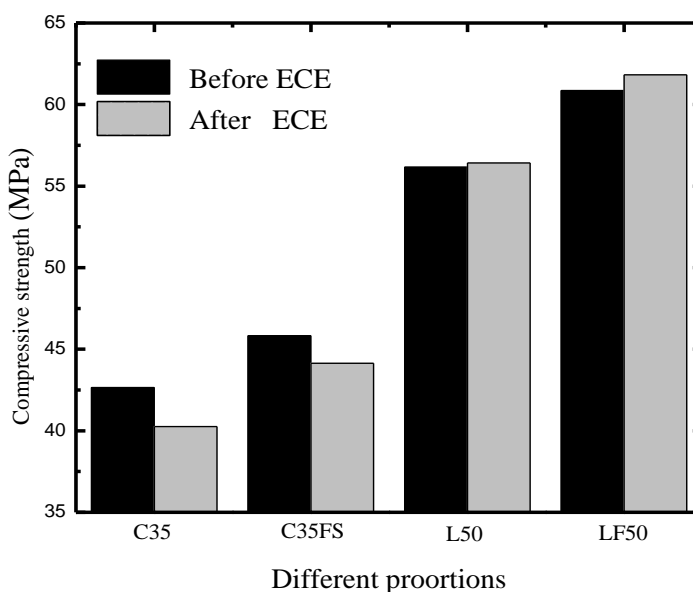


**Figure 9.** Compressive strength of concrete before and after ECE

The microstructure of C35 specimens at a depth of 2 mm, 22 mm and 42 mm from the steel bars as analysed by SEM are shown in Figure 10.

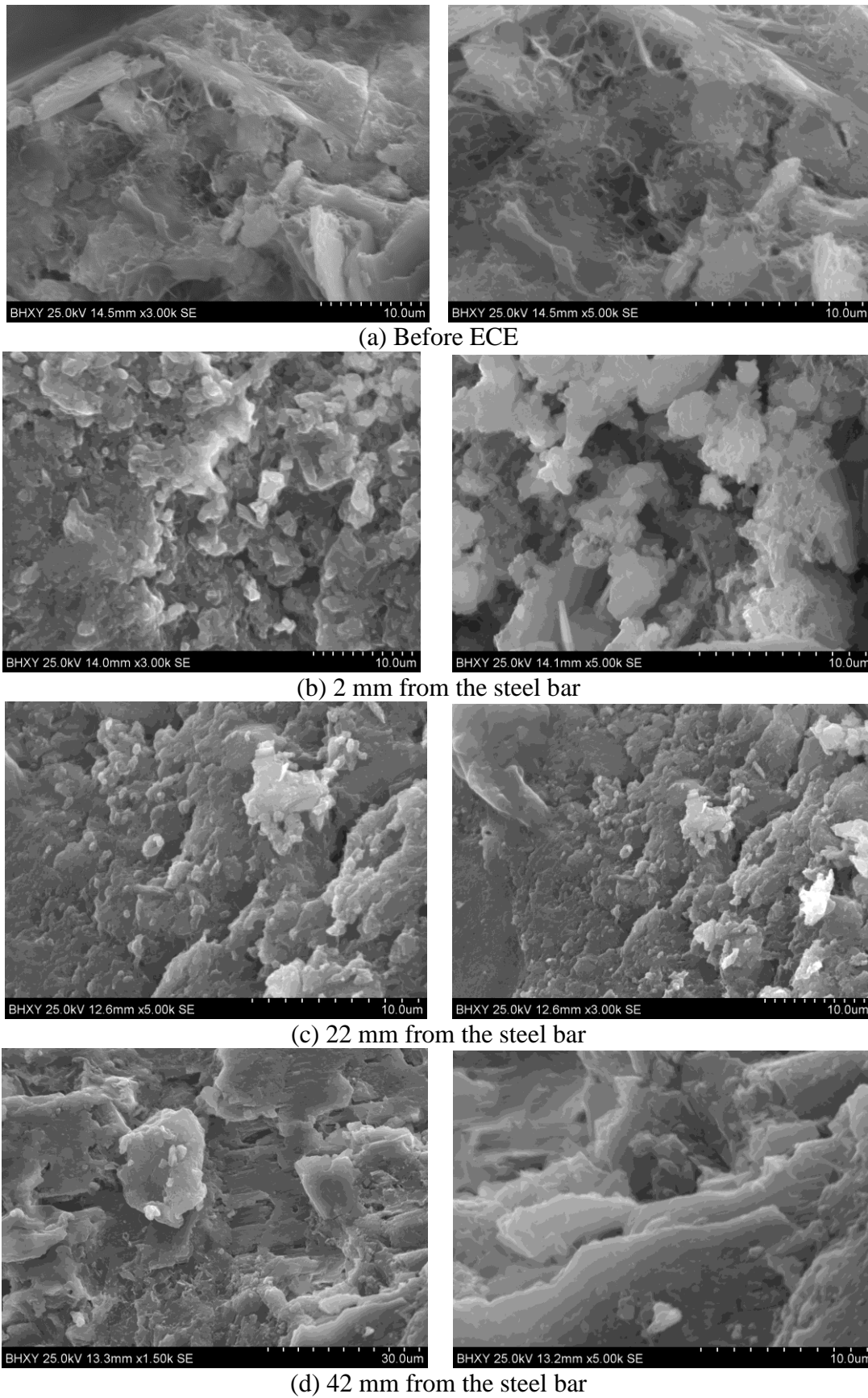


**Figure 10.** SEM images of microstructure evolution of concrete after ECE

Before ECE treatment, the microstructure of concrete was not compacted and porous due to expansion rust gathered on the interface zone between the steel bar and the concrete. After ECE treatment, some hexagonal plates of  $\text{Ca}(\text{OH})_2$  were observed, and the microstructure was compacted. In the middle area of the concrete, the damage induced by the ECE treatment was inconspicuous. On the concrete surface, the amounts of  $\text{Ca}(\text{OH})_2$  crystals could be observed because  $\text{OH}^-$  emerged from the ECE treatment to react with  $\text{Ca}^{2+}$  in the electrolyte solution.

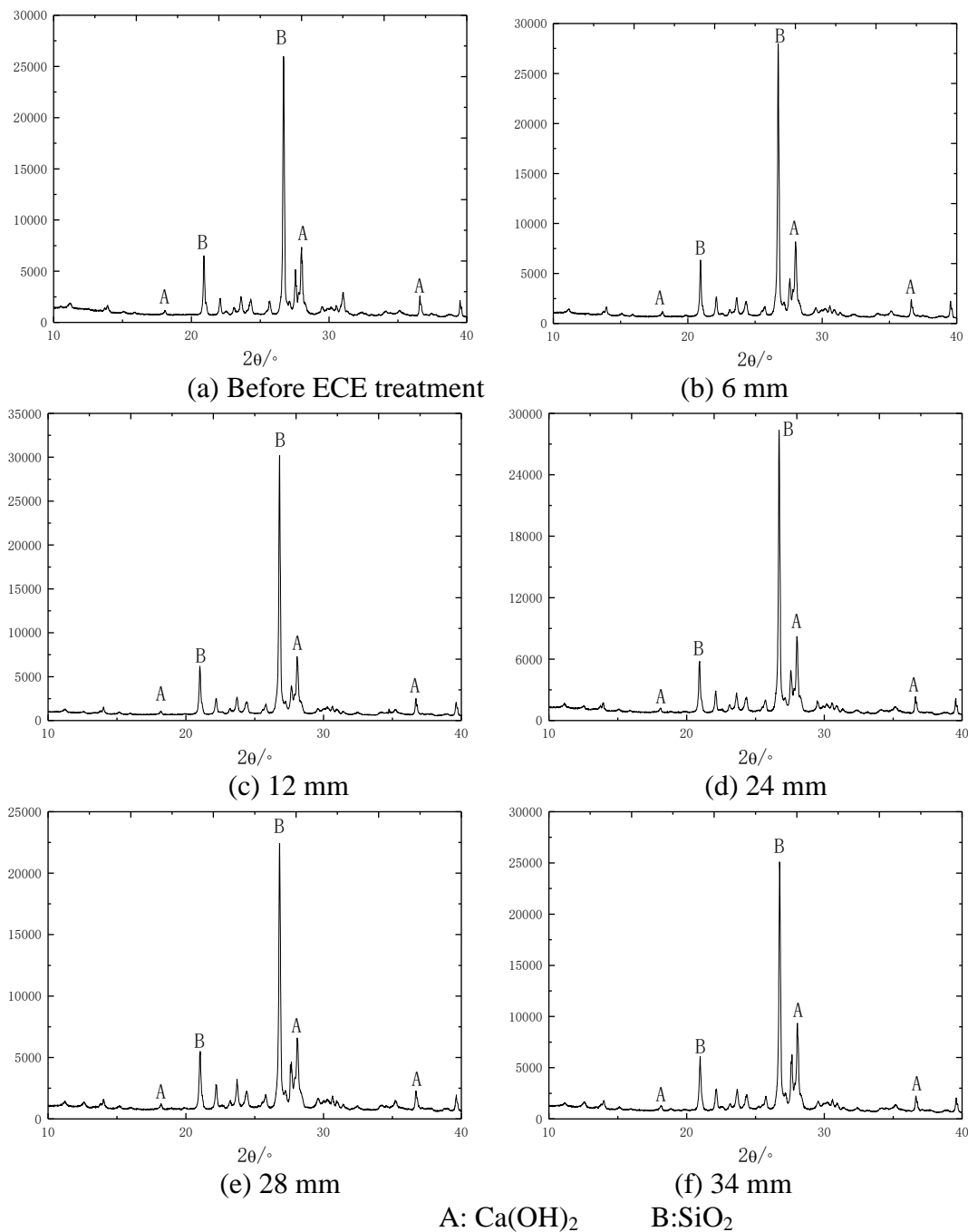
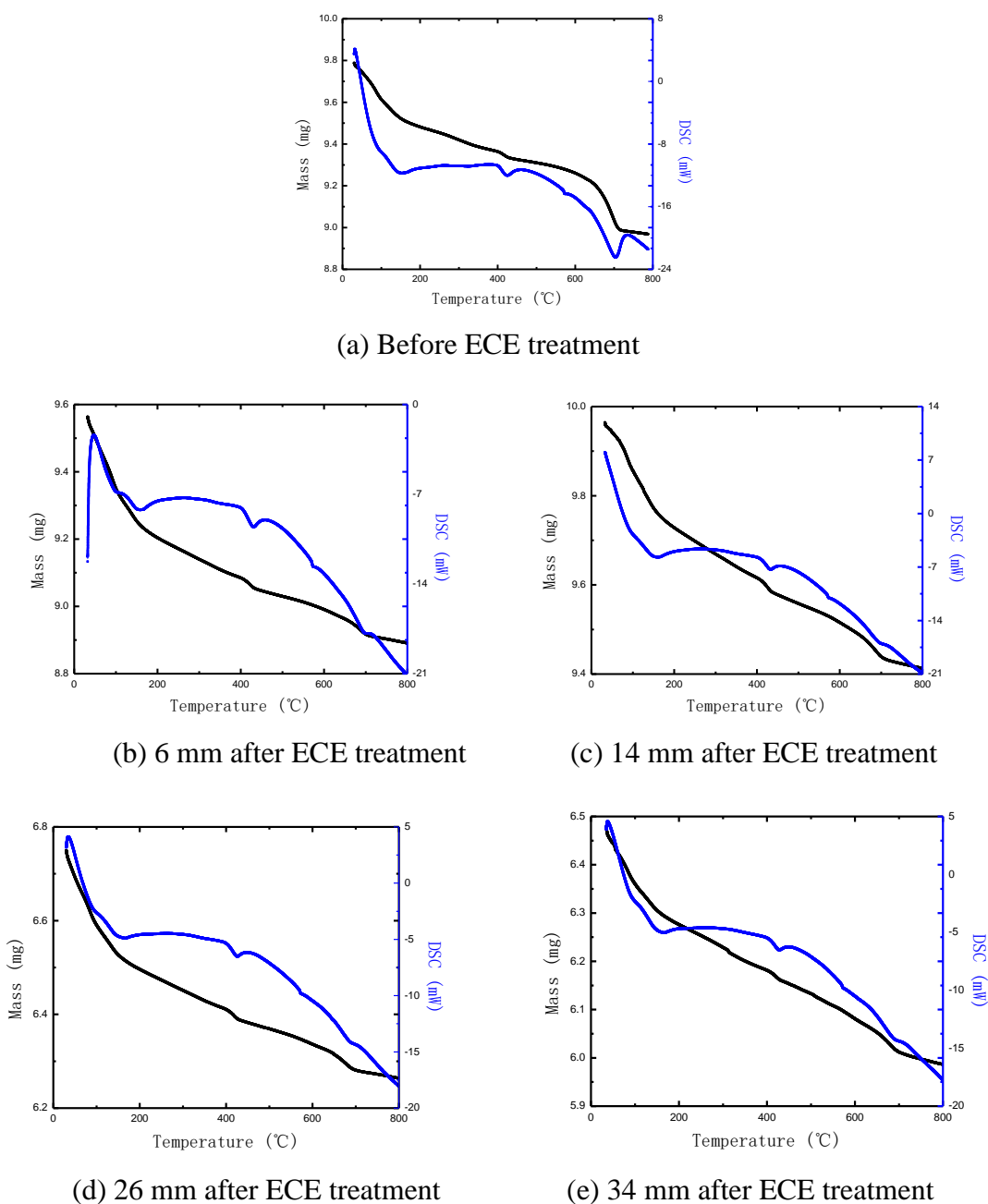


Figure 11. XRD Analysis of Different Areas of Concrete before and after ECE treatment

The hydration product evolution of concrete at depth of 6 mm, 12 mm, 24 mm, 28 mm and 34 mm was analysed by XRD and is plotted in Figure 11. The  $\text{Ca}(\text{OH})_2$  crystal characteristics of  $2\theta=18^\circ$  could be identified at different concrete depths.

The DSC-TG curves of the concrete before and after ECE treatment are demonstrated in Fig. 12. The endothermic peak of  $\text{Ca}(\text{OH})_2$  with  $T=400\sim 450^\circ\text{C}$  and the  $\text{CaCO}_3$  decomposition at  $T=700^\circ\text{C}$  can be observed in all the spectra.  $\text{CaCO}_3$  was mainly obtained from the carbonation of  $\text{Ca}(\text{OH})_2$  in the process of sample preparation. The  $\text{Ca}(\text{OH})_2$  content in different depths of the concrete was calculated and is illustrated in Figure 12 and Figure 13.



**Figure 12.** DSC-TG curves of concrete before and after ECE treatment

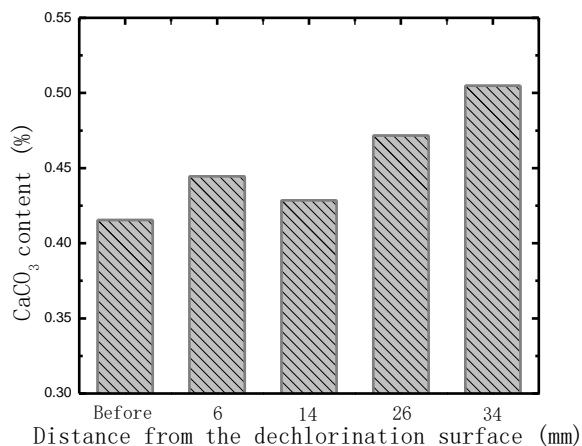


**Figure 13.** Content of Ca(OH)<sub>2</sub> in concrete before and after ECE treatment

The initial content of Ca(OH)<sub>2</sub> in concrete was approximately 0.41%. It increased with depth and was up to 0.50% at 34 mm from the surface. These hydration product evolution results indicated that the ECE treatment process repaired the microstructure near the steel bars.

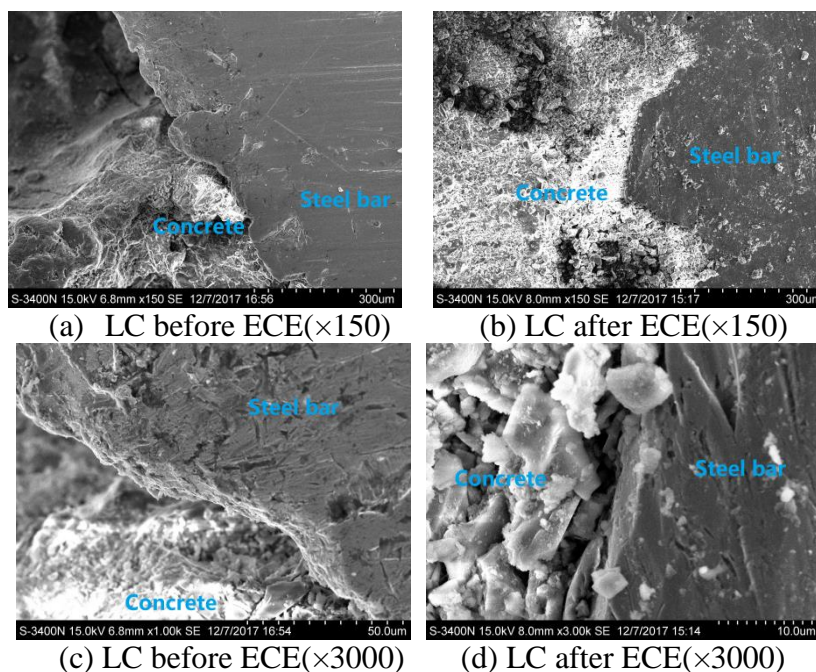


**Figure 14.** SEM images of the interface zone between the steel bar and the concrete before and after ECE

The microstructure of carbon-steel bars (LC) and corrosion-resistant steel bars (CR) in concrete after ECE treatment was observed by SEM, and the results are shown in Figure 14 and Figure 15, respectively. Before the ECE treatment, the steel bars were seriously damaged by corrosion, and many cracks could be observed on the edge of the bars. Cracks and voids could also be observed in the interface zone between steel bar and concrete due to expansion rust. After ECE, cracks near the

carbon-steel bars (LC) were repaired, and corrosion cracks could not be found on the corrosion-resistant steel bars (CR). A large amount of  $\text{Ca}(\text{OH})_2$  was deposited and compacted in the interface zone between the steel bars and the concrete.

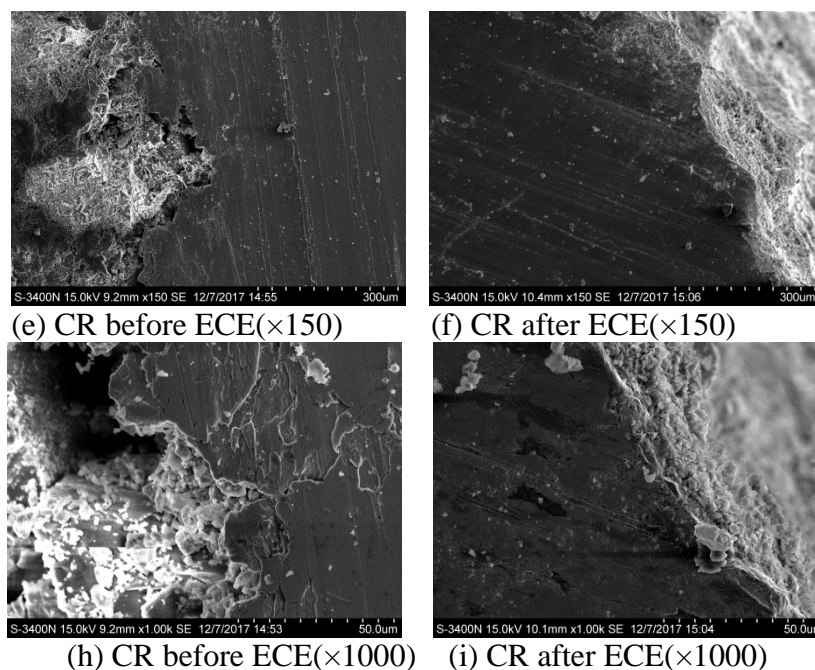


**Figure 15.** SEM images of the interface zone between the steel bar and the concrete before and after ECE

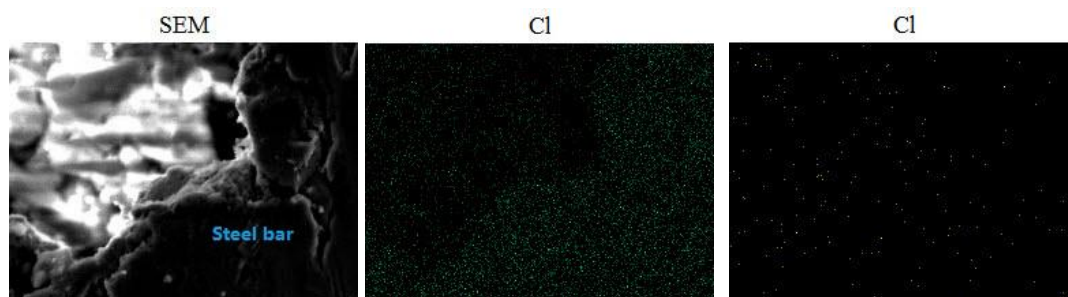


**Figure 16.** EDS images of Cl (green point) distribution from concrete to CR steel bar before and after ECE treatment

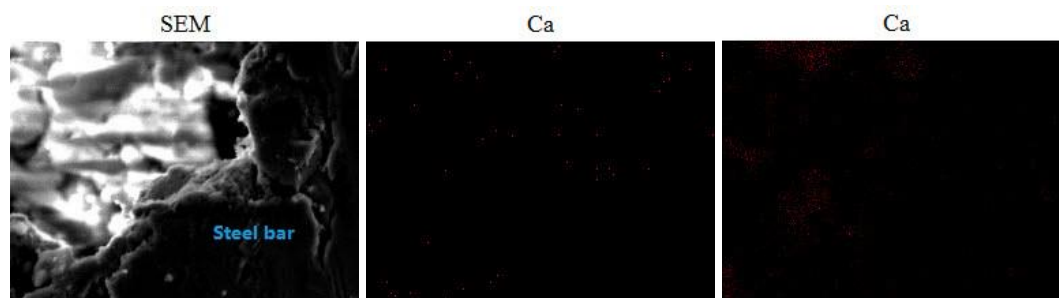


**Figure 17.** EDS images of Ca (red point) distribution from concrete to CR steel bar before and after ECE treatment

The Cl, Ca, K and Na elemental distribution from concrete to the steel bars was analysed by EDS, and the results are plotted in Figure 16-18. Before ECE treatment, many chloride ions were distributed in the concrete and steel bars. After ECE treatment, the chloride ion content in the concrete decreased sharply. Moreover, the chloride ion content was negligible near the steel bar. The accumulation of Ca, Na and K in the interface zone was observed more after the ECE treatment. Fajardo[38] also observed  $\text{Na}^+$ ,  $\text{K}^+$  and  $\text{Ca}^{2+}$  ions from the concrete pore solutions accumulated near the steel surface, and  $\text{K}^+$  ions moved towards the steel rebar more rapidly than the other cations did. Therefore, the interface between the concrete and steel bars could be repaired due to the high-pH recovery and deposition of  $\text{Ca}(\text{OH})_2$  as a result of ECE treatment.

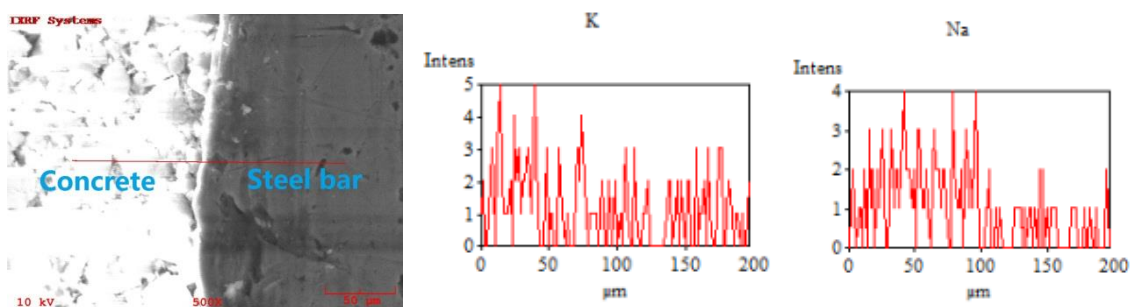


**Figure 18.** EDS images of K and Na elemental distribution from the concrete to the CR steel bars after ECE treatment

The microstructure results of concrete are similar to those found in previous studies. Xu[13] and Monteiro[39] found that if the chloride ion content was reduced below the critical threshold and  $\text{OH}^-$  was generated constantly near the cathodic reaction, the favourable environment assisted in the restoration of the reinforcement passivity.

#### 4. CONCLUSIONS

(1) The extracted chloride ion content from contaminated reinforced concrete decreased with time, and after 12 days of ECE treatment, the chloride ion content migration from concrete remained stable. However, a higher proportion of the chloride ions was accumulated at the middle of the concrete cover.

(2) When ECE treatment was performed with a stainless steel mesh as the anode, higher current densities resulted in higher chloride ion removal efficiencies. The best current density was  $2 \text{ A/m}^2$ , and saturated  $\text{Ca}(\text{OH})_2$  as an electrolyte solution was recommended when reinforced concrete was mixed with a non-active aggregate.

(3) A thicker concrete cover and more compacted concrete decreased the chloride ion removal efficiency. The influence of different types of steel bars on the concrete ECE treatment efficiency is very slight.

(4) After ECE treatment,  $\text{Ca}(\text{OH})_2$  deposited on the interface zone between the concrete and the steel bars, and  $\text{Na}^+$  and  $\text{K}^+$  migrated from the outer to the inner layers. Therefore, re-passivation of

steel bars was observed due to the pH recovery and dense microstructure induced by the ECE treatment.

#### ACKNOWLEDGMENTS

This investigation is funded by Chinese National Natural Science Foundation (NSF) Grant No. 51378269, 51678318 and No.51420105015, as well as the Chinese National 973 project Grant No. 2015CB655100. In addition, this work has also been supported by Chinese 111 plan. All these supports are gratefully appreciated.

#### References

1. X. Shi, N. Xie, K. Fortune and J. Gong, *Construction and Building Materials*, 30 (2012) 125.
2. J.X. Xu, Y.B. Song, L.H. Jiang, W. Feng, Y.L. Cao and W.W. Ji, *Construction and Building Materials*, 104 (2016) 9.
3. M.K. Moradillo, M. Shekarchi, M. Hoseini, *Construction and Building Materials*, 30 (2012)198.
4. H.Z. López-Calvo, P. Montes-Garcia, I. Kondratova, T.W. Bremner, M.D.A. Thomas, *Mater. Corros.*, 64 ( 2013) 599.
5. J.A. Jeong, C.K. Jin, W.S. Chung, *Journal of Advanced Concrete Technology*, 10 (2012) 389.
6. T. Bellezze, M. Malavolta, A. Quaranta, N. Ruffini and G. Roventi, *Cem. Concr. Compos.* 28 (2006) 246.
7. G. Ebell, A. Burkert, J. Lehmann and J. Mietz, *Mater. Corros.*, 63 (2012) 791.
8. I.M.A. Abuawad, L.L. Al-Oadi, I.S. Trepanier, *Construction and Building Materials*,84 (2015) 437.
9. N. Mohamed, M. Boulfiza and R. Evitts. *Journal of Materials Engineering and Performance*, 22 (2013) 787.
10. Z.Y. Ai, Corrosion behavior of new alloy corrosion-resistant steel and its anticorrosion mechanism(Doctoral thesis), *Southeast University*, (2017)Nanjing, China.
11. J.C. Orellan, G. Escadeillas and G. Arliguie, *Cem. Concr. Res.*, 34 (2004) 227.
12. A. Pérez, M.A. Climent and P. Garcés, *Corros., Sci.*, 52 (2010) 1576.
13. H. Shan, J. Xu, Z. Wang, L. Jiang and N. Xu, *Construction and Building Materials*, 127 (2016) 344.
14. A. Cañón, P. Garcés and M.A. Climent, *Corros. Sci.*, 77 (2013) 128.
15. L. Rodrigo de Almeida Souzaa, M. Henrique Farias de Medeirosa and E. Pereira, *Construction and Building Materials*, 145 (2017) 435.
16. VeluSaraswathy, Han-SeungLee, S. Karthick, *Construction and Building Materials*, 158 (2018) 549.
17. X. Shi, J. D. Cross, L. Ewan and Y. Liu, Replacing Thermal Sprayed Zinc Anodeson Cathodically Protected Steel Reinforced Concrete Bridges, *Journal of the Transportation Research Board*, 4 (2013) 56.
18. S.J. Bullard, B.S. Covino Jr and G Holcomb, *Corrosion*, 14 (1997) 9.
19. S.J. Bullard, B.S. Covino Jr and S.D. Cramer, *Corrosion*, 4 (1996) 40.
20. R. Brousseau, B. Arsenault and S. Dallaire, *Journal of Thermal Spray Technology*, 7 (1998) 193.
21. S.D. Cramer, B.S. Covino Jr and G.R. Holcomb, *Journal of Thermal Spray Technology*, 8 (1999) 133.
22. Z.G. Shao, F. Zhu and W.F. Lin, *Int. J. Electrochem. Soc.*, 153 (2006) 1575.
23. M.A. Petersen, T.C. Sale, K.F. Reardon, *Chemosphere*. 67 (2007) 1573.

24. P. Garces, E. Zornoza, E.G. Alcocel, *Construction and Building Materials*, 34 (2012) 91.
25. L. Bertolini, F. Bolzoni and T. Pastore, *Cem. Concr. Res.*, 34 (2004) 681.
26. J. Orlikowski, S. Cebulski and K. Darowicki, *Cem. Concr. Compos.*, 26 (2004) 721.
27. M. Siegwart, J.F. Lyness and F.J. Mc Farland, *Cem. Concr. Res.*, 33 (2003) 1211.
28. B. Elsener and U. Angst, *Corros. Sci.*, 49 (2007) 4504.
29. M. Sánchez, M.C. Alonso, *Construction and Building Materials*, 25 (2011) 873.
30. T. Marcotte, C. Hansson and B. Hope, *Cem. Concr. Res.*, 29 (1999) 1555.
31. B. Zhang, W. Gan and T. Chen, *Tumu Gongcheng Xuebao*, 39 (2006) 72.
32. T. Zhao, Z. Jin, M. Wang and J. Zhao, *Chinese Journal of Rock Mechanics and Engineering*, 26 (2007) 3823.
33. C. Yu, X. Mo and M. Deng, *Journal of Southeast University (Natural Science Edition)*, 39 (2009) 127.
34. Y. Lv, Y. Zhu and D. Lu, *Journal of Nanjing University of Technology*, 24 (2002) 35.
35. Z.L. Wang, J.P. Si, Y.F. Wang and H.K. Lin, *Science Technology and Engineering*, 16 (2016) 291.
36. J.J. Chang, *Construction and Building Materials*, 17 (2003) 281.
37. M. Castellote, C. Andrade, C. Alonso, *Cem. Concr. Res.*, 30 (2000) 615.
38. G. Fajardo, G. Escadeillas and G. Arliguie, *Corros. Sci.*, 48 (2006) 110.
39. E.C.B. Monteiro, Electrochemical chloride extraction for rehabilitation of concrete structures with steel reinforcement corrosion (Doctoral thesis), University of São Paulo, (2012) São Paulo, Brazil.